

# Dynamical Screening Effect on Local Two-Particle Vertex Functions

Li Huang<sup>1,2</sup> and Yilin Wang<sup>3</sup>

<sup>1</sup>*Science and Technology on Surface Physics and Chemistry Laboratory,  
P.O. Box 718-35, Mianyang 621907, Sichuan, China*

<sup>2</sup>*Department of Physics, University of Fribourg, Fribourg CH-1700, Switzerland*

<sup>3</sup>*Beijing National Laboratory for Condensed Matter Physics,  
and Institute of Physics, Chinese Academy of Sciences, Beijing 100190, China*

(Dated: June 27, 2021)

In principle, the electronic Coulomb interaction among the correlated orbitals is frequency-dependent. Though it is generally believed that the dynamically screened interaction may play a crucial role in understanding the subtle electronic structures of strongly correlated materials, hitherto we know very little about it. In the Letter, we demonstrate that within the framework of single-site dynamical mean-field theory the local two-particle Green's functions  $\chi$  and vertex functions  $\Gamma$  are strongly modified by the dynamically screened interaction. Since both  $\chi$  and  $\Gamma$  represent the main ingredients to compute momentum-resolved response functions and to treat non-local spatial correlations by means of diagrammatic extensions of dynamical mean-field theory, it is urgent to reexamine previous results by taking the dynamical screening effect into account. The modifications should be very considerable.

PACS numbers: 71.27.+a, 71.10.-w, 71.15.-m, 71.30.+h

Over the last years, tremendous progresses have been made in the studies of strongly correlated materials by using the density functional theory (DFT) combined with the dynamical mean-field theory (DMFT).[1, 2] The underlying physics in these materials can be generally captured by effective Hamiltonian models which are derived in the DFT calculations. Subsequently, these models are solved numerically or analytically in the DMFT part to extract various one-particle and two-particle quantities, which are used to compare with the corresponding experimental results if available.[3]

In classical DFT + DMFT calculations, the electron-electron interactions among the correlated orbitals are usually modeled by Coulomb interaction matrix which is parameterized with Hubbard  $U$ . It is hardly surprising that the calculated results rely heavily on the style of Hubbard  $U$ . [3] Usually  $U$  is assumed to be static. However, the charge density fluctuation in correlated orbitals will induce electric fields, which will be screened by the higher-lying or lower-lying states in the systems. The screening effect will finally result in a frequency-dependent renormalization for the Coulomb interaction. Thus, in principle the Coulomb interaction is dynamical, i.e.,  $U = U(\omega)$ . [4, 5] Since the dynamical screening effect may exist in strongly correlated materials widely, how to treat it is one of the major challenges in studying the intriguing properties of these materials. Due to many technical difficulties, it has been completely neglected or empirically taken into account by adjusting the static value  $U_0 = U(\omega = 0)$  [3] or reducing the effective bandwidth of correlated orbitals [6] in most calculations. Very recently, numerous efforts have been made to explore the dynamical screening effect in strongly correlated materials, [7–10] but very little is known on the consequences of frequency-dependent Coulomb interac-

tion. So far the only thing we can confirm is that the dynamical screening effect may play an essential role in understanding the fascinating properties of strongly correlated materials, [11, 12] such as the plasmon satellites and spectral weight transfer in the photoemission spectra of  $\text{SrVO}_3$  [13, 14] and hole-doped  $\text{BaFe}_2\text{As}_2$ , [15] which are less emphasized before.

The local two-particle vertex functions represent a crucial ingredient for the calculations of (momentum-dependent) dynamical susceptibilities, such as spin density wave, optical conductivity, thermopower, and thermal conductivity, etc. [16–22] Remarkably, it is argued that the local vertex functions can be used to calculate the electric polarization in correlated insulators [23] and to identify the fingerprints of Mott-Hubbard metal-insulator transition. [24] Beyond that, the local two-particle vertex functions are also the prerequisites for the diagrammatic extensions of the DMFT, such as the dynamical vertex approximation (D $\Gamma$ A) [25, 26] and dual fermion (DF) [27] approach, which aiming at the inclusion of non-local spatial correlations. Therefore, to obtain reliable and accurate local two-particle vertex functions is one of the major tasks in DMFT calculations all the time. However, though many numerical tricks and approximations were developed in recent years, [19–21] it is still higher difficulty and heavier workload of performing calculations at the two-particle level than the one-particle level. As a result it is not astonished that the analysis of two-particle quantities is usually restricted to the easiest cases of optical conductivity, for which one can neglect the vertex correction and retain the bubble term only, and then the calculation can be simplified to one-particle level eventually. [1–3]

In this Letter, we calculate and analyze the local two-particle Green's functions  $\chi$  and vertex functions  $\Gamma$

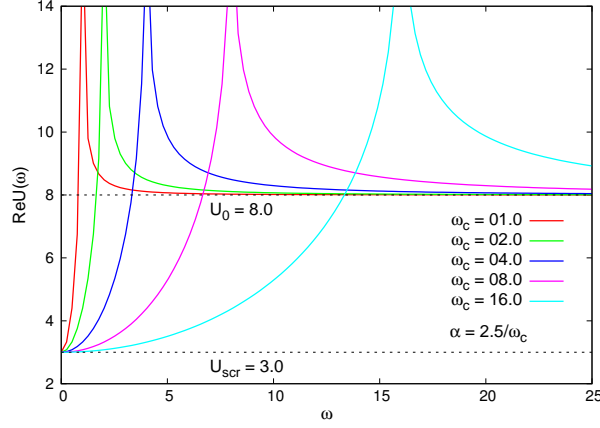


FIG. 1. (Color online) The typical Ohmic models used in the present calculations for frequency-dependent Coulomb interaction  $\text{Re}U(\omega)$ . The  $U_0$  and  $U_{\text{scr}}$  are fixed to 8.0 eV and 3.0 eV, respectively.

for single-band Hubbard model and strongly correlated metal  $\text{SrVO}_3$  by using the DMFT and DFT + DMFT approaches[1–3] respectively. The dynamical screening effects for both the Hubbard model and realistic materials are considered on the same footing in our calculations. We found that the calculated results for both  $\chi$  and  $\Gamma$  are significantly affected by the dynamically screened  $U$ . Therefore, it is suggested that the previous results and conclusions, concerning with the momentum-resolved response functions and diagrammatic extensions of DMFT, etc., should be reexamined and reconsidered carefully, provided that the dynamical screening effect is sizable and can not be ignored completely.

We now illustrate the analytical Ohmic model[7] which

is often used to describe the dynamically screened behaviour for Hubbard  $U$  :

$$\text{Re}U(\omega) = U_0 + \alpha\omega \ln \left| \frac{\omega_c + \omega}{\omega_c - \omega} \right| - 2\alpha\omega_c, \quad (1)$$

where  $\alpha$  and  $\omega_c$  are the screening parameters,  $U_0$  is the static interaction, and the screened interaction can be defined as  $U_{\text{scr}} = U_0 - 2\alpha\omega_c$ . Note that a characteristic feature of  $U(\omega)$  of paramagnetic Ni can be captured by this Ohmic model.[4, 5] Several typical Ohmic models used in the present calculations are shown in Fig.1. In order to include the dynamical screening effect into the DMFT and DFT + DMFT frameworks,[8–10] the hardest obstacle has been the lack of a reliable and efficient quantum impurity solver for the general impurity model with a frequency-dependent Coulomb interaction  $U(\omega)$ . Fortunately, it seems that this obstacle has been overcome by the recent development of hybridization expansion continuous-time quantum Monte Carlo impurity solver (dubbed CT-HYB) proposed by Werner *et al.*,[7, 8] where a multi-plasmon Lang-Firsov transformation is treated exactly in the context of a hybridization expansion algorithm for the general impurity model.

According to the literatures,[21, 22] the general two-particle Green's function  $\chi$  can be defined as follows:

$$\chi_{abcd}(\tau_a, \tau_b, \tau_c, \tau_d) = \langle T_\tau c_a(\tau_a) c_b^\dagger(\tau_b) c_c(\tau_c) c_d^\dagger(\tau_d) \rangle. \quad (2)$$

Generally these functions are evaluated in frequency space, as a function of two fermionic frequencies ( $\nu$  and  $\nu'$ ) and one bosonic frequency ( $\omega$ ). Then the local two-particle vertex functions  $\Gamma_{\sigma\sigma'}^{\nu\nu'\omega}$  can be derived directly by  $\chi_{\sigma\sigma'}^{\nu\nu'\omega}$  through the following equation:

$$\chi_{\sigma\sigma'}^{\nu\nu'\omega} = -\beta G_\sigma(\nu) G_\sigma(\nu + \omega) \delta_{\nu\nu'} \delta_{\sigma\sigma'} - G_\sigma(\nu) G_\sigma(\nu + \omega) \Gamma_{\sigma\sigma'}^{\nu\nu'\omega} G_{\sigma'}(\nu') G_{\sigma'}(\nu' + \omega), \quad (3)$$

where  $\beta$  is inverse temperature. We calculate the  $\chi_{\sigma\sigma'}^{\nu\nu'\omega}$  and  $\Gamma_{\sigma\sigma'}^{\nu\nu'\omega}$  with single-site DMFT and DFT + DMFT methods by using the powerful CT-HYB quantum impurity solver.[28, 29] An improved estimator for  $\chi_{\sigma\sigma'}^{\nu\nu'\omega}$  suggested by Hafermann *et al.*[19, 21] is adopted to suppress the numerical noises and yield accurate data.

For the sake of simplicity, above all we consider a half-filled one-band Hubbard model on the Bethe lattice with bandwidth  $4t$  at  $\beta = 50.0$ . The static and screened Hubbard  $U$  are 8.0 eV and 3.0 eV, respectively. Then we tune the  $\alpha$  and  $\omega_c$  parameters for the Ohmic model to monitor the variational trends for selected one-particle quantities and local two-particle vertex functions.

(a) *Dynamical screening effect on spin-spin correlation function and local magnetic moment in one-band Hubbard model.* Previous studies show that the dynamically

screened interaction can shift the metal-insulator phase boundary,[7] change the spectral function near the Mott-Hubbard gap edge, and renormalize the quasiparticle band structure.[13, 14] Inspired by these works, we study the spin-spin correlation function  $\chi_{\text{ss}}(\tau) = \langle S_z(0) S_z(\tau) \rangle$  in the Hubbard model with frequency-dependent  $U$  to gain more insight into the dynamical screening effect. The obtained  $\chi_{\text{ss}}(\tau)$ , effective local magnetic moment  $M_e = \sqrt{T \chi_{\text{ss}}}$ , and quasiparticle weight  $Z$  are shown in Fig.2. As is seen in this figure, the  $\chi_{\text{ss}}(\tau)$ ,  $M_e$ , and  $Z$  are strongly modulated by the screening frequency parameter  $\omega_c$  of the Ohmic model. Obviously, there exists a critical  $\omega_c$  separating the metal and Mott insulator phases. We just focus on the following two cases: (i) The screening frequency  $\omega_c$  is small ( $\omega_c \leq 4.0$ ). The  $\chi_{\text{ss}}(\tau)$  approaches a non-zero constant at large times

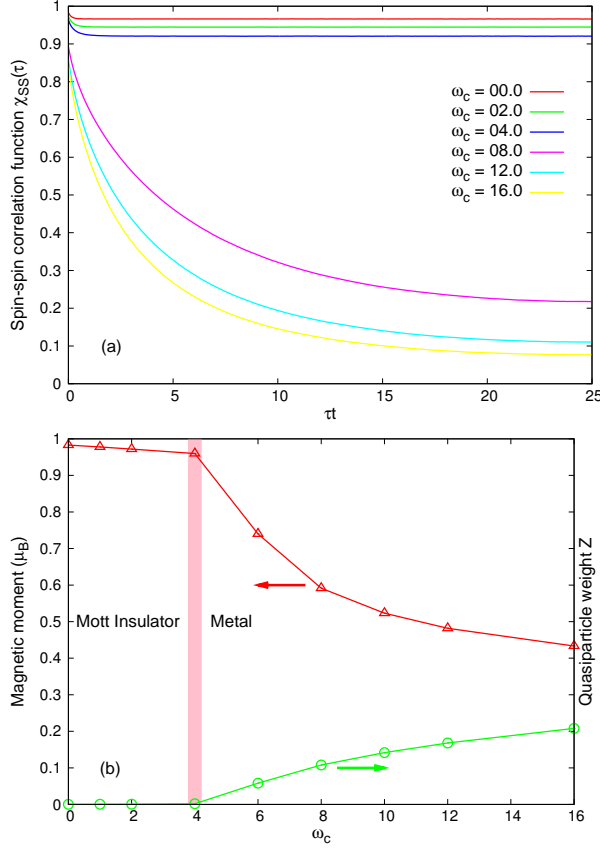


FIG. 2. (Color online) Magnetic moment collapse and metal-insulator transition in half-filled one-band Hubbard model induced by the dynamical screening effect. (top) Spin-spin correlation function  $\chi_{SS}(\tau) = \langle S_z(0)S_z(\tau) \rangle$ . (bottom) Quasiparticle weight  $Z$  and local spin magnetic moment  $\sqrt{T}\chi_{SS}$  as a function of  $\omega_c$ . The Mott metal-insulator transition zone is highlighted by a pink vertical bar.

which characterizes a frozen moment phase.  $M_e$  only decreases slightly from its initial value (0.98  $\mu_B$  at  $\omega_c = 0.0$ ) under the increment of  $\omega_c$ . And the quasiparticle weight  $Z$  approximates zero, which means the system should exhibit completely insulating properties. (ii) The screening frequency  $\omega_c$  is large ( $\omega_c > 4.0$ ). The behavior of  $\chi_{SS}(\tau)$  manifests that the system still retains the frozen moment phase. Whereas,  $M_e$  decreases quickly and monotonously from 0.96  $\mu_B$  to 0.43  $\mu_B$ , i.e., the effective local magnetic moment appears apparent collapse. On the other hand, the quasiparticle weight  $Z$  becomes more and more considerable when  $\omega_c$  increases, which means that the system goes into a fully metallic state. Further analysis on the imaginary part of the calculated low-frequency Matsubara self-energy function  $\text{Im}\Sigma(i\omega)$  indicates that it exhibits noticeably fractional power-law behavior with respect to  $i\omega$ , which is the signature of the non-Fermi-liquid metallic phase. In Fig.2, we observe a sudden drop for  $M_e$  and rise for  $Z$  around  $\omega_c = 4.0$ , which corresponds to a typical first-order transition.

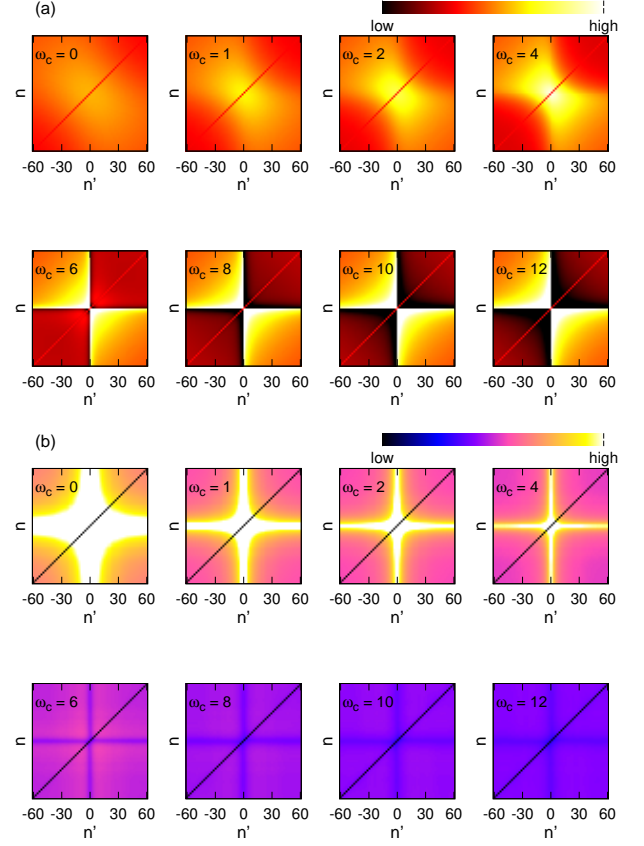


FIG. 3. (Color online) Vertex functions vs. the two fermionic frequencies  $\nu = (2n+1)\pi/\beta$  and  $\nu' = (2n'+1)\pi/\beta$  as a function of the screening frequency  $\omega_c$  for half-filled single-band Hubbard model. (top) Real part of spin-up-up component for the local two-particle Green's functions:  $\text{Re}\chi_{\uparrow\uparrow}^{\nu\nu'\omega}$ . (bottom) Real part of spin-up-up component for the local two-particle vertex functions:  $\text{Re}\Gamma_{\uparrow\uparrow}^{\nu\nu'\omega}$ . Note that the bosonic frequency  $\omega$  is fixed to be zero. Instead of the absolute values of the Matsubara frequencies just the corresponding indexes are given so as to improve the readability of these figures.

(b) *Dynamical screening effect on local two-particle vertex functions in one-band Hubbard model.* We then concentrate our attentions to the local two-particle Green's functions  $\chi_{\sigma\sigma'}^{\nu\nu'\omega}$  and full vertex functions  $\Gamma_{\sigma\sigma'}^{\nu\nu'\omega}$ . In Fig.3, only the contour maps for their spin-up-up components (the bosonic frequency  $\omega = 0$ ) are displayed. As is clear in this figure, if the dynamical screening effect is included in the DMFT calculations, not only the one-particle quantities but also the two-particle quantities are modified visibly, which are not taken seriously before. Let's look at the  $\text{Re}\chi_{\uparrow\uparrow}^{\nu\nu'\omega}$  part (see top panel in Fig.3) at first. The intensity plots of it can be divided into two kinds. (i) For  $\omega_c \leq 4.0$ , one observes a gradual enhancement at the low-frequency zone (central area). But neither the singularity nor obvious geometric structures is detected. (ii) For  $\omega_c > 4.0$ , a numerical divergence emerges at  $\nu \rightarrow 0$  and  $\nu' \rightarrow 0$  zone, where the intense

white-black color coding indicates alternating signs in the  $(\nu, \nu')$  space. This low-frequency divergence becomes more and more prominent when  $\omega_c$  increases steadily. In addition, one can distinguish two “cone”-like structures easily which are totally absent when  $\omega_c \leq 4.0$ . Next we pay attention to the  $\text{Re}\Gamma_{\uparrow\uparrow}^{\nu\nu'\omega}$  part (see bottom panel in Fig.3). The most striking features in the contour plots is the cross structure. Interestingly, the vertices can be split into two types based on the intensity and sign of the cross structures as well. (i) For  $\omega_c \leq 4.0$ , the cross structure is notable and positive. Upon increasing the screening frequency  $\omega_c$ , the intensity weakens and the extent shrinks. (ii) For  $\omega_c > 4.0$ , the cross structure exists too, but its sign is now inverted as indicated by the colors. In other words, the cross structures are concave, contrary to those in the  $\omega_c \leq 4.0$  case. Furthermore, the vertex tends to be featureless with the increment of  $\omega_c$ . Thus, it is suggested that the frozen moment phase with large local magnetic moment will strengthen the two-particle vertex functions  $\Gamma$ , which is in accord with the previous results obtained by Hafermann *et al.*[21] They found that the vertex is essentially featureless on the Fermi liquid side, and evident in the frozen moment phase. To make a long story short, dramatic changes will occur in both the intensity and structure of  $\text{Re}\chi_{\uparrow\uparrow}^{\nu\nu'\omega}$  and  $\text{Re}\Gamma_{\uparrow\uparrow}^{\nu\nu'\omega}$ , accompanying with the first-order metal-insulator transition and collapse of local magnetic moment, when the screening frequency  $\omega_c$  approaches the critical point. We also make detailed analysis on the other components or channels for  $\chi$  and  $\Gamma$ , and the other reducible and irreducible vertex functions.[22] They exhibit analogous features when the dynamical screening effect is activated.

(c) *Dynamical screening effect on local two-particle vertex functions in SrVO<sub>3</sub>.* So far all the discussions are limited to the simplest single-band Hubbard model, and the frequency-dependent interaction  $U$  is modeled by analytical Ohmic model.[7] In order to confirm the above conclusions, we conduct further DFT + DMFT calculations for strongly correlated metal SrVO<sub>3</sub> to examine the consequences of dynamical screening effect on the two-particle Green’s functions and vertex functions. SrVO<sub>3</sub> is an ideal system to benchmark the new theories and tools describing the strongly correlated materials. It has been the subject of numerous experimental and theoretical studies.[3] In previous works, several DFT + DMFT calculations were devoted to study the one-particle quantities of SrVO<sub>3</sub> under the dynamical screening effect.[6, 10, 13, 14] It is shown to renormalise the spectral weight near the Fermi level, to increase the effective mass, and to suppress the  $t_{2g}$  quasiparticle bandwidth distinctly. Nevertheless, to our knowledge, the two-particle quantities of SrVO<sub>3</sub> have not been studied before neither experimentally nor theoretically. So our results can be regarded as a valuable prediction.

The frequency-dependent interaction for realistic materials can be evaluated at the random phase approxi-

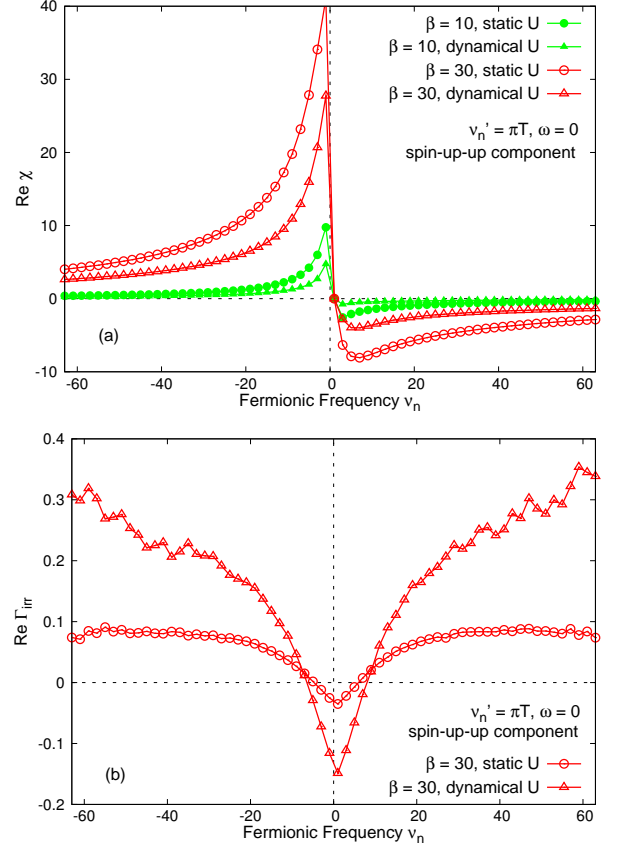


FIG. 4. (Color online) Real part of the spin-up-up component of vertex functions for strongly correlated metal SrVO<sub>3</sub> obtained in the DFT + DMFT calculations. (top) Local two-particle Green’s functions  $\text{Re}\chi_{\sigma\sigma'}^{\nu\nu'\omega}$ . (bottom) Local irreducible vertex functions  $\text{Re}\Gamma_{\text{irr}}$ . The second fermionic frequency  $\nu'$  is fixed to be  $\pi T$ , and the bosonic frequency  $\omega$  is set to be zero. The static  $U$  is 4.0 eV, and the data for frequency-dependent  $U$  are taken from reference [5] directly. The DFT + DMFT calculations are done for  $\beta = 10$  and  $\beta = 30$ , respectively.

mation (RPA) level as usual. As for SrVO<sub>3</sub>, the  $U(\omega)$  data are taken from reference [5] directly. The details for our DFT + DMFT calculations can be found in reference [14]. The main calculated results, real part of spin-up-up component of local two-particle Green’s function  $\text{Re}\chi_{\sigma\sigma'}^{\nu\nu'\omega}$ , are shown in the top panel of Fig.4. Comparing the calculated results with and without dynamical interaction, the difference is rather significant, especially for the  $\nu \rightarrow 0$  region. Moreover, the difference is amplified at lower temperature. When the dynamical screening effect is included, the absolute values of  $\text{Re}\chi_{\sigma\sigma'}^{\nu\nu'\omega}$  are strongly reduced. Similar or opposite trends are found for the other two-particle vertex functions, such as the local irreducible vertex functions  $\Gamma_{\text{irr}}$  (see the bottom panel of Fig.4). The vertices  $\Gamma_{\text{irr}}$  can be evaluated straightforward through the famous Bethe-Salpeter equation:  $\Gamma_{\text{irr}} = \beta(\chi_0^{-1} - \chi^{-1})$ , where the polarization bubble

$\chi_0$  is computed from the fully interacting one-particle Green's function.[22]

Finally, it should be stressed that in many strongly correlated materials, the dynamical screening effect is conspicuous.[4, 5] Werner *et al.*[15] have demonstrated that the fine electronic structures of hole-doped  $\text{BaFe}_2\text{As}_2$  can be fully understood only if the dynamical screening effect is taken into account for the first time. Recently, Park *et al.*[17] have studied the magnetic excitation spectra in  $\text{BaFe}_2\text{As}_2$  through a two-particle approach within standard DFT + DMFT framework. Their calculated results, including the local irreducible vertex  $\Gamma_{\text{irr}}$ , dynamic magnetic susceptibility  $\chi(\mathbf{q}, i\omega)$ , and dynamical structure factor  $S(\mathbf{q}, \omega)$ , roughly reproduced all the experimentally observed features in inelastic neutron scattering.[30] Since in their calculations just the static interaction was used, we believe that incorporating the dynamical screening effect into the DFT + DMFT calculations will contribute to improving their results.

In summary, we study several typical one-particle and two-particle quantities in both the half-filled single-band Hubbard model and transition metal oxide  $\text{SrVO}_3$  by applying the DMFT and DFT + DMFT methods with frequency-dependent interaction  $U$ . In the case of the Hubbard model, the dynamical screening effect is shown to drive first-order metal-insulator transition and magnetic moment collapse by tuning the screening parameter  $\omega_c$  of the Ohmic model. The intensity and structure for both the local two-particle Green's functions  $\chi_{\sigma\sigma'}^{\nu\nu'\omega}$  and full vertex functions  $\Gamma_{\sigma\sigma'}^{\nu\nu'\omega}$  display dramatic changes when the critical  $\omega_c$  is attained. Concerning the strongly correlated metal  $\text{SrVO}_3$ , the calculated two-particle vertex functions are also suppressed or enhanced by the dynamical screening explicitly. Enormous changes for the  $\mathbf{q}$ -dependent response functions are expected. Anyway, the two-particle quantities in either Hubbard model or realistic materials are intensively affected by the dynamical screening effect. Hence, in future studies with regards to moment-resolved response functions and diagrammatic extensions of DMFT, careful considerations for the dynamical screening effect should be essential.

We acknowledge financial support from the National Science Foundation of China and by the 973 program of China (No.2013CBP21700 and No.2011CBA00108). All of the DMFT and DFT + DMFT calculations have been performed on the TIANHE-1A at National Supercomputing Center of Tianjin (NSSC-TJ).

- 
- [1] A. Georges, G. Kotliar, W. Krauth, and M. J. Rozenberg, *Rev. Mod. Phys.* **68**, 13 (1996).  
 [2] G. Kotliar, S. Y. Savrasov, K. Haule, V. S. Oudovenko, O. Parcollet, and C. A. Marianetti, *Rev. Mod. Phys.* **78**, 865 (2006).

- [3] V. Anisimov and Y. Izyumov, *Electronic Structure of Strongly Correlated Materials*, Springer Series in Solid-State Sciences, Vol. 163 (Cambridge University Press, 2012).  
 [4] F. Aryasetiawan, M. Imada, A. Georges, G. Kotliar, S. Biermann, and A. I. Lichtenstein, *Phys. Rev. B* **70**, 195104 (2004).  
 [5] F. Aryasetiawan, K. Karlsson, O. Jepsen, and U. Schönberger, *Phys. Rev. B* **74**, 125106 (2006).  
 [6] M. Casula, P. Werner, L. Vaugier, F. Aryasetiawan, A. Millis, and S. Biermann, (2012), arXiv:1204.4900 [cond-mat].  
 [7] P. Werner and A. J. Millis, *Phys. Rev. Lett.* **104**, 146401 (2010).  
 [8] P. Werner and A. J. Millis, *Phys. Rev. Lett.* **99**, 146404 (2007).  
 [9] F. F. Assaad and T. C. Lang, *Phys. Rev. B* **76**, 035116 (2007).  
 [10] M. Casula, A. Rubtsov, and S. Biermann, *Phys. Rev. B* **85**, 035115 (2012).  
 [11] T. Ayral, P. Werner, and S. Biermann, *Phys. Rev. Lett.* **109**, 226401 (2012).  
 [12] T. Ayral, S. Biermann, and P. Werner, (2012), arXiv:1210.2712 [cond-mat].  
 [13] J. M. Tomczak, M. Casula, T. Miyake, F. Aryasetiawan, and S. Biermann, *Europhys. Lett.* **100**, 67001 (2012).  
 [14] L. Huang and Y. Wang, *Europhys. Lett.* **99**, 67003 (2012).  
 [15] P. Werner, M. Casula, T. Miyake, F. Aryasetiawan, A. J. Millis, and S. Biermann, *Nat. Phys.* **8**, 331337 (2012).  
 [16] L. Boehnke and F. Lechermann, *Phys. Rev. B* **85**, 115128 (2012).  
 [17] H. Park, K. Haule, and G. Kotliar, *Phys. Rev. Lett.* **107**, 137007 (2011).  
 [18] N. Lin, E. Gull, and A. J. Millis, *Phys. Rev. Lett.* **109**, 106403 (2012).  
 [19] L. Boehnke, H. Hafermann, M. Ferrero, F. Lechermann, and O. Parcollet, *Phys. Rev. B* **84**, 075145 (2011).  
 [20] J. Kuneš, *Phys. Rev. B* **83**, 085102 (2011).  
 [21] H. Hafermann, K. R. Patton, and P. Werner, *Phys. Rev. B* **85**, 205106 (2012).  
 [22] G. Rohringer, A. Valli, and A. Toschi, *Phys. Rev. B* **86**, 125114 (2012).  
 [23] R. Nourafkan and G. Kotliar, (2013), arXiv:1303.0764 [cond-mat].  
 [24] T. Schäfer, G. Rohringer, O. Gunnarsson, S. Ciuchi, G. Sangiovanni, and A. Toschi, (2013), arXiv:1303.0246 [cond-mat].  
 [25] C. Slezak, M. Jarrell, T. Maier, and J. Deisz, *J. Phys.: Condens. Matter* **21**, 435604 (2009).  
 [26] A. Toschi, A. A. Katanin, and K. Held, *Phys. Rev. B* **75**, 045118 (2007).  
 [27] A. N. Rubtsov, M. I. Katsnelson, and A. I. Lichtenstein, *Phys. Rev. B* **77**, 033101 (2008).  
 [28] P. Werner, A. Comanac, L. de' Medici, M. Troyer, and A. J. Millis, *Phys. Rev. Lett.* **97**, 076405 (2006).  
 [29] E. Gull, A. J. Millis, A. I. Lichtenstein, A. N. Rubtsov, M. Troyer, and P. Werner, *Rev. Mod. Phys.* **83**, 349 (2011).  
 [30] M. Liu, L. W. Harriger, H. Luo, M. Wang, R. A. Ewings, T. Guidi, H. Park, K. Haule, G. Kotliar, S. M. Hayden, and P. Dai, *Nat. Phys.* **8**, 376 (2012).